Multimodal Image-Guided Photothermal Therapy Mediated by ^{188}Re-Labeled Micelles Containing a Cyanine-Type Photosensitizer

Cheng-Liang Peng,[†,‡] Ying-Hsia Shih,[‡] Pei-Chi Lee,[†] Thomas Mon-Hsian Hsieh,[†] Tsai-Yueh Luo,[‡,*] and Ming-Jium Shieh[†,§,*]

[†]Institute of Biomedical Engineering, College of Medicine and College of Engineering, National Taiwan University, No. 1, Section 1, Jen-Ai Road, Taipei 100, Taiwan, [‡]Isotope Application Division, Institute of Nuclear Energy Research, P.O. Box 3-27, Longtan, Taoyuan 325, Taiwan, and [§]Department of Oncology, National Taiwan University Hospital and College of Medicine, #7, Chung-Shan South Road, Taipei 100, Taiwan

ABSTRACT Multifunctional micelles loaded with the near-infrared (NIR) dye and labeled with the radionuclide rhenium-188 (^{188}Re) have been developed to provide multimodalities for NIR fluorescence and nuclear imaging and for photothermal therapy (PTT) of cancer. The NIR dye, IR-780 iodide, allowed the micelles to have dual functions in cancer NIR imaging and PTT. The ^{188}Re-labeled IR-780 micelles enabled imaging by NIR fluorescence and by microSPECT to guide the delivery of drugs and to monitor in real-time the tumor accumulation, intratumoral distribution, and kinetics of drug release, which serve as a basis of specific photothermal injury to the targeted tissue. We also investigated the biodistribution, generation of heat, and photothermal cancer ablation of IR-780 micelles of both *in vitro* and *in vivo* xenografts. Histopathology observed irreversible tissue damage, such as necrotic features, decreased cell proliferation, increased apoptosis of cells, and increased expression of heat shock proteins in the PTT-treated tumors. The ^{188}Re-labeled IR-780 micelles offer multifunctional modalities for NIR fluorescence and nuclear imaging and for PTT of cancer.

KEYWORDS: photothermal therapy (PTT) · IR-780 iodide · near-infrared (NIR) fluorescence imaging · radiopharmaceuticals · rhenium-188 (^{188}Re) · microSPECT/CT imaging

Photothermal therapy (PTT) destroys cancer cells by generating heat within a tumor by absorbing specific light sources.[1,2] A major challenge of thermal therapies is to selectively injure the targeted tissue without damaging the normal tissue. Minimally invasive cancer treatments are currently being investigated, such as radiofrequency ablation,[3] magnetic thermal ablation,[4] focused ultrasound ablation,[5] and laser-based PTT.[6,7] The effectiveness of such treatments is limited by nonspecific heating of targeted tissue, which often injures healthy tissue.[8] Since exogenous chromophores increase the light sensitivity of the targeted tissue to PTT, it offers the advantage of being a precisely targeted treatment. Its use of selective illumination can be repeated in the same site if necessary, and it is less invasive than surgery.

Such exogenous chromophores as gold nanoparticles (NPs),[9,10] gold nanorods,[11−13] gold nanoshells,[1] and organic chromophores[14] like indocyanine green (ICG)[15−17] increase heat generation within targets by increasing the light sensitivity of targeted tissue. Therefore, exogenous chromophores that strongly absorb light in the near-infrared (NIR) region (650−900 nm) have been widely studied because they produce localized cytotoxic heat upon NIR irradiation. Since the tissue absorption of NIR light is minimal, it can penetrate deep into the tissue.[18,19]

Polymethine cyanine dyes such as indocyanine green (ICG), IR-783, and IR-780 iodide are suitable contrast agents for clinical and experimental NIR imaging.[20−22] ICG also exhibits unique optical properties due to its strong absorption at NIR wavelengths, which causes photothermal effects that can trigger thermal injury and cell death both *in vitro* and *in vivo*.[15−17] The IR-780 iodide is a lipophilic cation dye with peak absorption at 780 nm that can be conveniently detected by a NIR fluorescent detection system,[22] but it is virtually insoluble in all pharmaceutically acceptable solvents. To overcome its solubility problem, we examined delivering it by micelles to determine if IR-780 iodide could be used for *in vivo* experiments and clinical uses.

Polymeric nanoparticles, which include micelles composed of amphiphilic block copolymers, have shown great promise in drug delivery.[23−26] Polymeric micelles have demonstrated good biocompatibility, high stability both *in vitro* and *in vivo*, and

* Address correspondence to soloman@ntu.edu.tw, tylo@iner.gov.tw.

Received for review March 23, 2011 and accepted June 14, 2011.

Published online June 14, 2011
10.1021/nn201100m

successful encapsulation of various poorly soluble agents. In our previous study, chlorin-core star-shaped block copolymer (CSBC) self-assembled to encapsulate such hydrophobic drugs as paclitaxel,[27] SN-38,[28] and the photosensitizer mTHPC.[29] An additional benefit of nanosized carriers is that they slowly accumulate in pathological sites, including tumors, through the enhanced permeability and retention (EPR) effect, which is known as a "passive" targeting.[30] Many tumor tissues are supplied by a leaky neovasculature with an incomplete endothelial barrier and poor lymphatic drainage. The EPR phenomenon provides an opportunity for nanosized carriers to reach their target site.

Incorporating radionuclides into micelles has been investigated for noninvasive biodistribution studies that produce images through single photon emission computed tomography (SPECT)[31,32] or positron emission tomography (PET).[33] Nuclides frequently used for this purpose are $^{99\,m}$Tc, ^{111}In, and ^{64}Cu because these isotopes are easily available, have straightforward labeling procedures, and have half-lives that allow for SPECT imaging.[34] Recently, rhenium-188 (^{188}Re, $t_{1/2}$ = 16.9 h) has emerged as a promising isotope for both therapeutic and diagnostic clinical purposes because it decays by β emission ($E_{\beta\text{-max}}$ = 2.12 MeV) and by 15% γ emission (E_{γ} = 155 KeV).[35]

In this study, we prepared multifunctional micelles for optical and nuclear imaging and for PTT. We incorporated two imageable components into this micelle, a NIR dye and a radionuclide, which created a multifunctional drug delivery system that permitted image-guided drug delivery and real-time monitoring of the accumulation of the drug in the tumor, the intratumoral distribution, and the kinetics of drug release. We demonstrated that IR-780 iodide-loaded micelles (IR-780 micelles), which were labeled with the radionuclide rhenium-188 (^{188}Re), can combine the modalities of targeting, imaging, and drug delivery on one nanocarrier. This multifunctional micelle presents simultaneous optical and nuclear imaging and treatment capacities in one delivery system, using NIR fluorescence imaging, microSPECT/CT imaging, and photothermal cancer ablation. The size and morphology of IR-780 micelles were determined by dynamic light scattering (DLS) and transmission electron microscopy (TEM), and their encapsulation efficiency and optical properties were also analyzed. Cellular cytotoxicity by the IR-780 micelles upon NIR irradiation was evaluated in human colon cancer HCT-116 cells, and a xenograft model of these cells investigated the biodistribution, SPECT imaging, generation of heat, and photothermal cancer ablation of IR-780 micelles.

RESULTS AND DISCUSSION

We synthesized mPEG-*b*-PCL and Fmoc-NH-PEG-*b*-PCL by a ring-opening polymerization of ε-caprolactone in the presence of either mPEG-OH or Fmoc-NH-PEG-OH, respectively (Figure 1). Both mPEG-*b*-PCL and Fmoc-NH-PEG-*b*-PCL were characterized by ^{1}H NMR spectrum, and the molecular weights and polydispersity of copolymers were determined by GPC.[27] The characteristics of mPEG$_{5k}$-PCL$_{10k}$, Fmoc-NH-PEG$_{5k}$-PCL$_{10k}$, and DTPA-PEG$_{5k}$-PCL$_{10k}$ are summarized in Table 1. The characteristic resonances of both PCL (δH^e = 1.37 ppm, δH^d = 1.65 ppm, δH^c = 2.28 ppm, δH^f = 4.07 ppm) and mPEG (δH^a = 3.39 ppm and δH^b = 3.65 ppm) were observed, suggesting the coexistence of two blocks. The molecular weight ($M_{n,NMR}$) of PCL was determined by comparing the peak intensities of the methylene protons of the oxyethylene units (δH^b) of mPEG to the methylene protons (δH^d) of PCL (details in the Supporting Information Figure SI-1).[27] This molecular weight (MW) was in good agreement with the theoretical MW that was calculated based on the feed ratio of ε-CL to mPEG or Fmoc-NH-PEG.

The ^{1}H NMR spectrum of Fmoc-NH-PEG-*b*-PCL exhibited distinct resonance signals of Fmoc moieties at 7.30−7.76 ppm, which were not present in the spectrum of mPEG-*b*-PCL (Supporting Information Figure SI-1). Analysis by GPC revealed a shift to earlier elution times for Fmoc-NH-PEG-*b*-PCL, relative to Fmoc-NH-PEG-OH, which is consistent with an increase in MW distribution and indicates a successful ring-opening polymerization of ε-CL. The Fmoc-NH-PEG-*b*-PCL copolymer had a slight broadening of the GPC peaks and polydispersity compared to the Fmoc-NH-PEG macroinitiator (Supporting Information Figure SI-2).

Amino-terminated PEG-*b*-PCL (H_2N-PEG-*b*-PCL) copolymers were prepared *via* deprotection of the Fmoc-NH-PEG-*b*-PCL that was accomplished by stirring Fmoc-NH-PEG-*b*-PCL with 20% piperidine in DMF as previously described.[36] The NH_2-PEG-*b*-PCL copolymers were then purified by dialysis before being lyophilized to dryness. The DTPA-PEG-*b*-PCL were prepared by conjugating the DTPA dianhydride with the amino group of N_2H-PEG-*b*-PCL as described previously.[37] The conjugation efficiency of DTPA dianhydride to NH_2-PEG-*b*-PCL was evaluated by ITLC that analyzed the efficiency of the ^{188}Re labeling of DTPA-PEG-*b*-PCL. It revealed that 76.8% of the radioactivity remaining at the origin corresponded to ^{188}Re -DTPA-PEG-*b*-PCL (Supporting Information Figure SI-3.). The copolymer MW of DTPA-PEG-*b*-PCL was determined to be ~14 000 Da by ^{1}H NMR spectroscopy and ~15 100 Da by GPC (Table1).

The IR-780-loaded micelles, as observed by TEM, had a spherical morphology with particle sizes in agreement with DLS (Figure 2). The mPEG-*b*-PCL micelles had a size distribution about 100 nm in diameter smaller than previously reported.[27] After IR-780 was loaded into micelles using various D/P ratios, DLS determined that the micelles ranged from 155 to 203 nm in size with various polydispersity indices (Table 2). Those IR-780-loaded micelles with a D/P ratio of 1:20 were

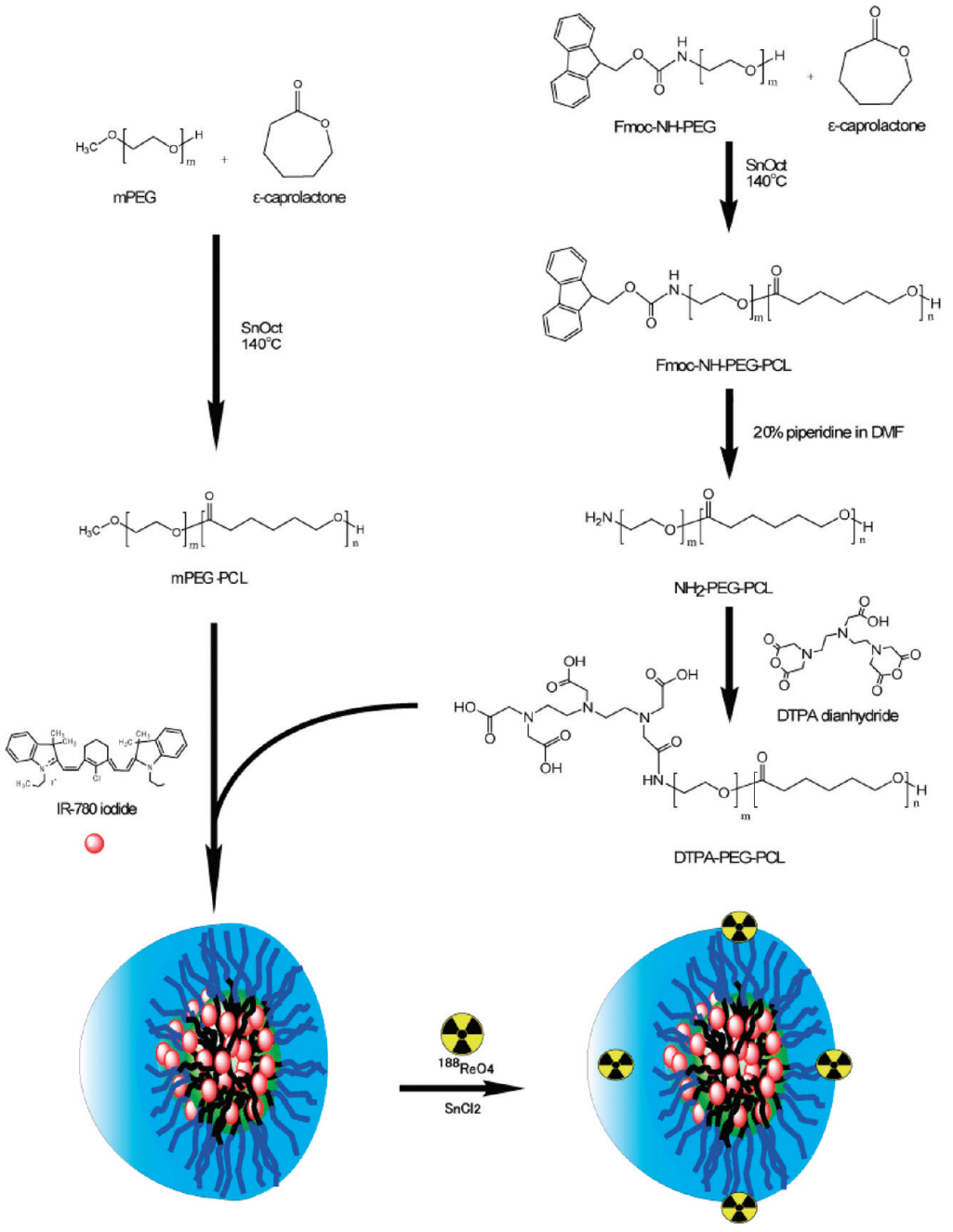

Figure 1. Schematic diagram illustrates the fabrication of ^{188}Re-labeled IR-780 iodide-loaded micelles.

TABLE 1. Characteristics of mPEG-*b*-PCL and DTPA-PEG-*b*-PCL Copolymers

sample	$M_{n,Theo}$ [a]	$M_{n,NMR}$ [b]	$M_{n,GPC}$ [c]	M_w/M_n [c]	CMC [d] (wt %)	size [e] (nm)
$mPEG_{5k}$-*b*-PCL_{10k}	15000	15400	20900	1.31	0.006	74 ± 32
Fmoc-NH-PEG_{5k}-*b*-PCL_{10k}	15000	14200	15900	1.28		
DTPA-PEG_{5k}-*b*-PCL_{10k}		14000	15100	1.42		

[a] Theoretical molecular weight based on feed ratio. [b] Calculated from ^{1}H NMR data. [c] Determined by GPC. [d] CMC indicates critical micelle concentration. [e] As determined by DLS.

employed, which had an encapsulation efficiency of 93.8%, and each micelle contained approximately 6414 ± 641 IR-780 iodide dye molecules (details are presented in Supporting Information). The micelles with a D/P ratio of 1:5 or 1:10 had larger particle sizes and lower encapsulation efficiencies than those with a D/P ratio of 1:20 (Table 2). Drug encapsulation efficiency is a crucial factor in developing micelles or other drug delivery vesicles. Moreover, since a drug solution will be distributed all over the body, the EPR effect may preferentially distribute nanoparticles of 100−300 nm to the tumor,[38,39] while the reticuloendothelial system will readily scavenge drug carriers with a diameter larger than 200 nm.[40,41] The IR-780 micelle with a D/P ratio of 1:20, which exhibited efficient drug encapsulation and

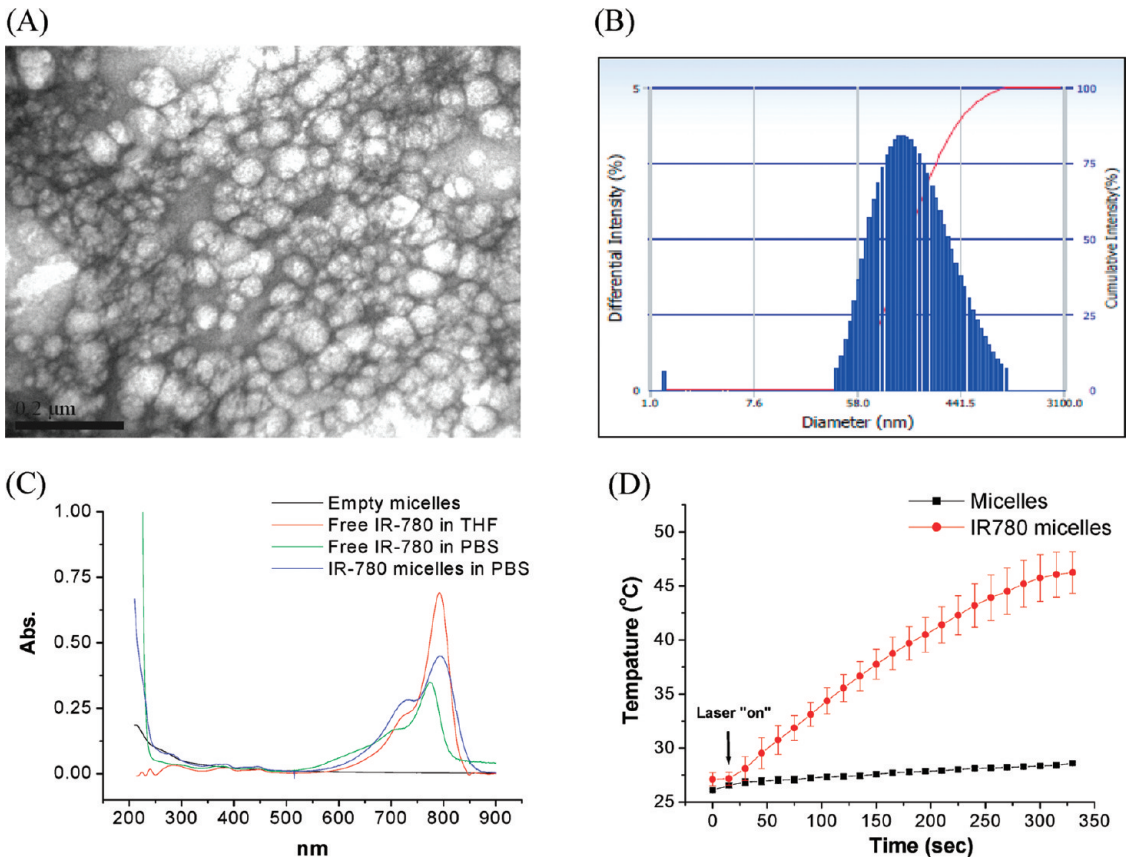

Figure 2. Characterization of IR-780 micelles. (A) IR-780 micelles were imaged by TEM, and the scale bar is 200 nm. (B) Size distribution of IR-780 micelles at a D/P ratio of 1:10 was analyzed by DLS. (C) Absorbance spectra were measured for empty micelles, free IR-780 iodide, and IR-780 micelles in PBS. (D) Temperature of IR-780-loaded micelles during 1.8 W/cm^2 NIR laser irradiation was profiled, with the data presented as mean ± SD.

TABLE 2. Characteristics of IR-780 Micelles

polymer	D/P ratio	encapsulation efficiency (%)[b]	drug content (%)[c]	mean size/nm (PDI)[d]
m52	1:5	30.3	5.71	203.6 (0.436)
	1:10	62.9	5.92	187.9 (0.317)
	1:20	74.8	3.61	143.8 (0.236)
m510	1:5	34.6	6.47	172.2 (0.367)
	1:10	63.3	5.95	165.7 (0.307)
	1:20	93.8	4.47	155.0 (0.293)

[a] D/P ratio = weight of IR-780 iodide/weight of polymer. [b] IR-780 iodide encapsulation efficiency (%) = (weight of IR-780 iodide in the micelles/weight of the feeding IR-780 iodide) × 100%. [c] IR-780 iodide drug content (%) = (weight of IR-780 iodide)/(weight of IR-780 iodide + weight of polymer) × 100%. [d] As determined by DLS.

an ideal size suitable for future medical applications, was chosen as the drug carrier for further study.

The IR-780 cyanine dye diluted in THF and IR-780 micelles in PBS strongly absorbed in the NIR region with a maximum wavelength (λ_{max}) at ~795 nm (Figure 2C). Since IR-780 cyanine dye is lipophobic, it aggregates in aqueous buffer. The aggregation of lipophilic IR-780 iodide results in a broad and blue-shifted absorption peak at λ_{max} = 775 nm (as shown in Figure 2C), which decreased the absorption from laser diode with a wavelength of 808 nm, resulting in reduced efficiency of PTT. In contrast, the IR-780-loaded micelles still exhibited a relatively strong absorbance in the NIR range in aqueous buffer, indicating that loading the lipophobic IR-780 cyanine dye in the micelles to encapsulate it did not change its photophysical properties, as has also been described elsewhere.[42] The temperature of the IR-780-loaded micelle medium increased rapidly during NIR irradiation and reached maximal temperature of approximately 46 °C after 5 min, while the empty micelles increased by 2.5 °C during NIR irradiation (Figure 2D). These results indicate that most of the heat during NIR irradiation came from the IR-780 dye.

The IR-780 iodide-loaded DTPA micelles (IR-780/DTPA micelles) were labeled with ^{188}Re by reacting IR-780/DTPA micelles, ^{188}Re-perrhenate, and stannous chloride for 2 h at 37 °C. The ^{188}Re-labeled IR-780/DTPA micelles had high radioactivity and radiochemical purity (~90%) as analyzed by ITLC (Supporting Information Figure SI-5.).

The heat generating capabilities of IR-780 micelles in PBS suspension were previously demonstrated, and here we used HCT-116 cells to evaluate the cytotoxicity

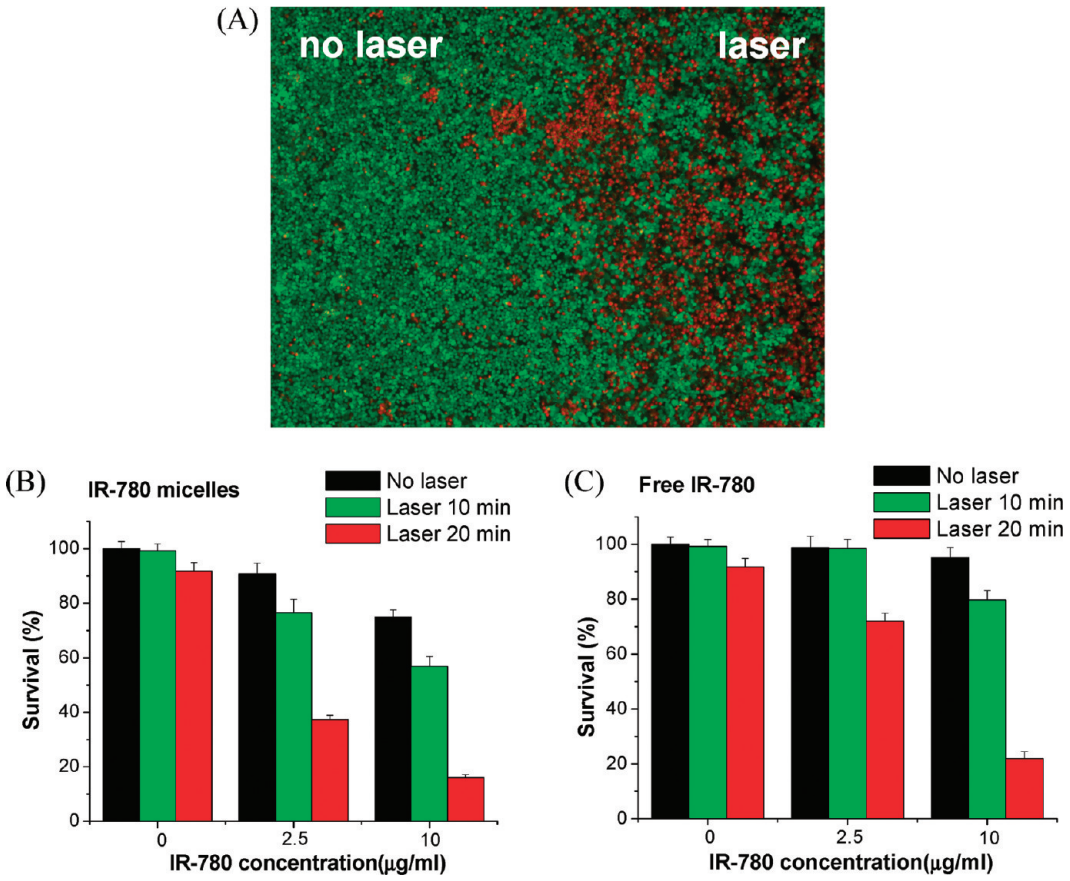

Figure 3. (A) Photothermal ablation and live/dead staining is illustrated for HCT-116 cells that were treated with 0.6 W/cm^2 NIR irradiation (treated region labeled "laser") for 10 min mediated by 10 μg/mL IR-780 micelles. The live cells are stained green with calcein-AM, and dead cells are stained red with PI. The cytotoxicities of IR-780 micelles (B) and free IR-780 iodide (C) in HCT-116 cells without or with 0.6 W/cm^2 NIR irradiation for 10 or 20 min.

of HCT-116 treated with IR-780 micelles plus NIR irradiation. The cells were treated with IR-780 micelles and NIR irradiation, and then live cells were stained with calcein AM, a nonfluorescent cell-permeating compound that is hydrolyzed by intracellular esterases in live cells into intensely fluorescent calcein, and dead cells with PI (Figure 3A). Live cells were determined by the green fluorescence of calcein in the dark region. The light regions indicated cell death, where increased PI penetration and binding to nucleic acids produced a bright red fluorescence. The increased loss of cell viability in the irradiated regions confirmed that cell death was confined to the area treated by the IR-780 micelles with NIR irradiation. Exposing the cells to IR-780 micelles without NIR irradiation did not compromise cell viability.

The cytotoxicity of IR-780 micelles and free IR-780 iodide in HCT-116 cells without or with NIR irradiation was also determined by the MTT assay. Treatment of the cells with only NIR irradiation for 10 or 20 min did not cause observation cell death (Figure 3B). Treatment with IR-780 micelles without irradiation had more toxicity than free IR-780 iodide in HCT-116 cells. However, we observed no systemic toxicity of IR-780 micelles in nude mice, and this formulation also did not significantly affect body weights of the mice compared with control groups (as shown in Figure 7B).

The HCT-116 cells treated with 2.5 μg/mL of IR-780 micelles and NIR irradiation (excess 14.4 and 53.5% of cells killed for 10 and 20 min of irradiation, respectively) significantly accelerates cell killing than that treated with 2.5 μg/mL of free IR-780 iodide and NIR irradiation (excess 0.3 and 26.8% of cells killed for 10 and 20 min of irradiation, respectively). The observation may be due to the aggregation of lipophilic IR-780 iodide in the aqueous medium, which reduces their photocytotoxicity and cellular uptake.[43] The aggregation of lipophilic IR-780 iodide shows a broad and blue-shifted absorbance spectrum with a peak at λ_{max} = 775 nm (as showm in Figure 2C), which decreased the absorbance for laser diode with a wavelength of 808 nm, resulting in reduced efficiency of PTT. When HCT-116 cells were treated with high concentrations and NIR irradiation, it showed significant phototoxicity by IR-780 micelles (85% of cells killed after 20 min of irradiation) compared with that by free IR-780 iodide. These results indicate that IR-780 micelles can be activated by 808 nm laser diode and act as a potential formulation for PTT.

The biodistribution of ^{188}Re-labeled IR-780 micelles was evaluated in tumor and normal tissues of mice

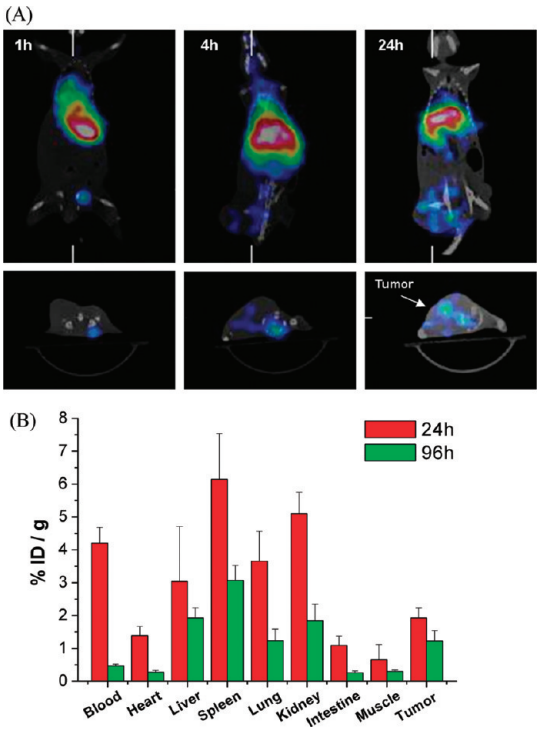

Figure 4. MicroSPECT/CT images and biodistribution of ^{188}Re-labeled IR-780 micelles in tumor mice bearing HCT-116 are illustrated. (A) ^{188}Re-labeled IR-780 micelles were injected, and then microSPECT/CT images were acquired 1, 4, and 24 h later. (B) ^{188}Re-labeled IR-780 micelles were intravenously injected into mice bearing HCT-116 tumors, and their biodistribution was determined 1, 4, 24, 48, and 72 h later. Each column represents the mean ± SD.

bearing HCT-116 human colon cancer xenografts. Images obtained by microSPECT/CT revealed that radioactivity accumulated in the spleen, liver, and tumor at 24 h after the injection of ^{188}Re-labeled IR-780 micelles, and that the tumors were targeted by the radioactivity (Figure 4A). Biodistribution of ^{188}Re-labeled IR-780 micelles was also performed by γ-counting. The results indicated that the ^{188}Re-labeled micelles were widely and rapidly distributed into most tissues and the tumors, with the highest accumulations occurring in the spleen, followed by liver, kidney, lung, and tumor at 24 h after injecting micelles (Figure 4B). After 96 h, the accumulation of radioactivity in all tissues and in the tumor decreased, with the spleen still having the highest radioactivity. This high radioactivity may be due to filtering by the splenic capillary bed that removed some large particles or their aggregates.[41] The percentage ID per gram of ^{188}Re-labeled micelles decreased slowly at the tumor site from 1.93 ± 0.30% ID/g at 24 h after the injection to 1.23 ± 0.31% ID/g at 96 h, and it decreased quickly in the blood and most tissues. The tumor to muscle ratio of ^{188}Re-labeled micelles increased from 1.91 ± 1.71 at 24 h after the injection to 4.27 ± 1.48 at 96 h, which corresponds well to the EPR effects of the nanoparticles. Thus, amphiphilic-block-copolymer-based micelles appear to be an ideal candidate carrier that can "passively" target tumors, which is an ability that may improve antitumor efficacy and reduce the toxicity to and nonspecific targeting of normal cells that accompanies most chemotherapy or PTT.[8,44]

We characterized the *in vivo* real-time biodistribution of IR-780 iodide in HCT-116 tumor-bearing mice that were injected intravenously with ^{188}Re-labeled IR-780 micelles through NIR fluorescence imaging with an IVIS imaging system. The IR-780 iodide had a time-dependent biodistribution and tumor accumulation in mice bearing HCT-116 tumors (Figure 5A). The whole bodies of the mice had clear NIRF signals during the first 24 h that decreased as time passed. The NIRF signals were visible in the tumor region for 96 h. We quantified the intensity of the NIRF signals in the tumor and normal chest regions and the contrast index (CI) values at various time points after the IR-780 micelles were injected (Figure 5B). The NIRF signal intensities of tumors gradually increased compared with the normal region after injections. The maximal NIRF signals in the nontumor regions of whole body were selected to calculate the CI. The CI values increased from 1.01 to 1.95 over the time course of the IR-780 micelle injections (Figure 5B), and the maximum CI values occurred 96 h after the injections, which is a result that favors the reduced skin phototoxicity and enhanced antitumor efficacy of cyanine-based PTT. The heart, liver, spleen, lung, kidneys, and intestine were isolated to evaluate the tissue distribution of IR-780 micelles by NIRF imaging 24 h after the IR-780 micelles were injected (Figure 5C), and their signals were quantified (Figure 5D). Because the lungs had higher concentrations of IR-780 iodide, the NIRF signals from the chest of mice were clearly visualized by whole body imaging during the experiment period (Figure 5A), which has also been found using gold nanorod−photosensitizer complexes for NIRF imaging.[45] Comparing the biodistribution of radioactivity from the ^{188}Re-labeled IR-780 micelles, which represent the biodistribution of the nanocarrier, the highest concentration of IR-780 iodide was detected in the lungs. This may result from filtering by the tissue capillary bed that ruptured the structure of the micelle and caused the drug to be released and redistributed to other organs.

We measured the intratumoral temperature profiles during PTT mediated by IR-780 micelles (Figure 6). Thermocouple needles were inserted in the center of tumor as a function of time, while the tumor region was irradiated by a 1.8 W/cm^2 NIR laser for 5 min. After the 5 min of NIR irradiation, the tumors treated with IR-780 micelles had a temperature increase of ~27 °C, which exceeds the damage threshold needed to induce irreversible tissue damage.[1] In contrast, the PBS-treated tumor for the same NIR irradiation resulted in a temperature increase of ~10 °C (Figure 6B), which is insufficient to irreversibly damage tissue.[1]

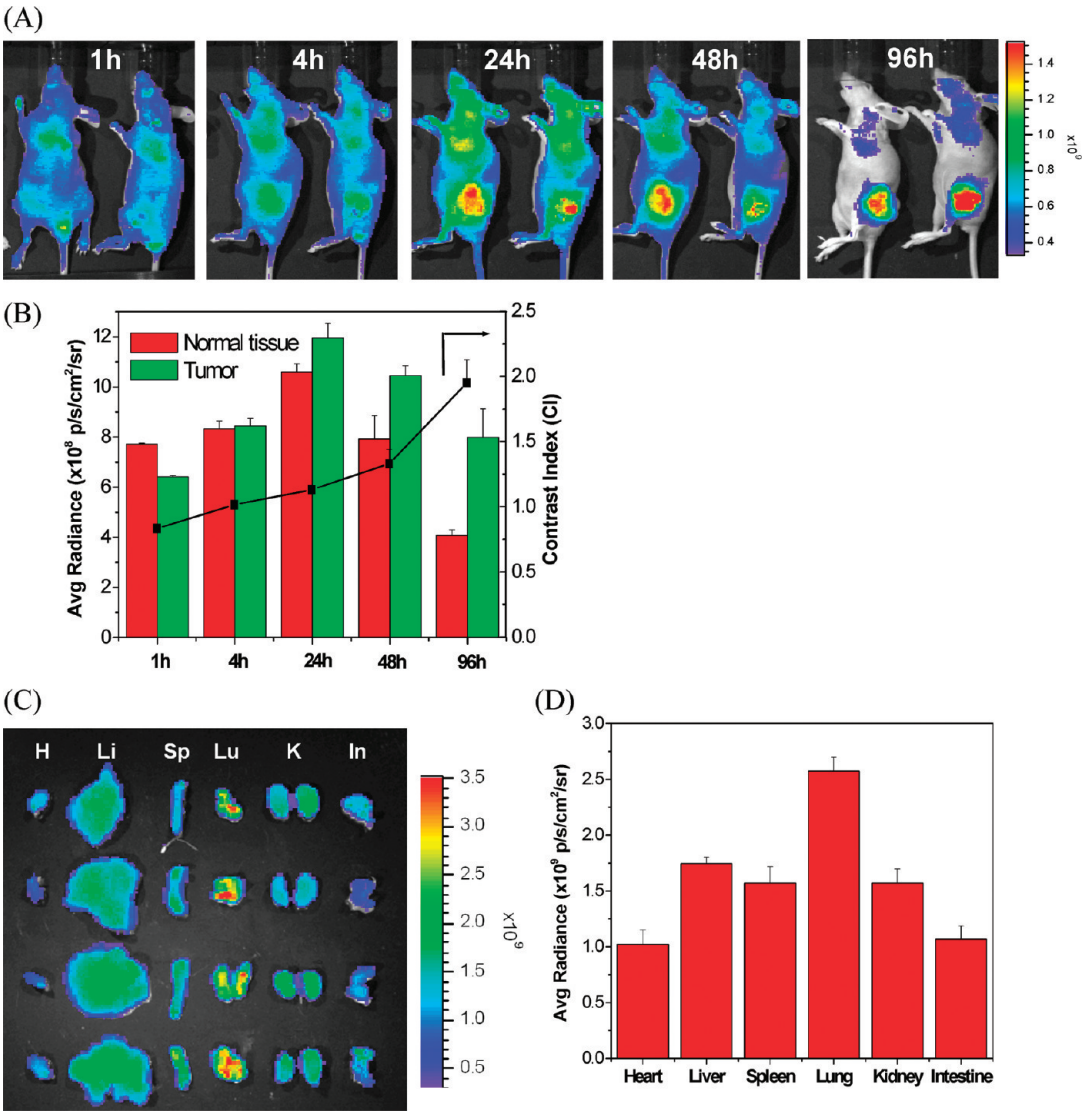

Figure 5. (A) Time-lapse near-IR fluorescence (NIRF) imaged mice bearing HCT-116 tumors after intravenous injections of IR-780 micelles. (B) NIR fluorescence intensities and contrast index (CI) values were quantified at the indicated time points in the tumor and normal regions, using the maximal NIRF signals in the nontumor regions. (C) Near-IR fluorescence (NIRF) images and (D) quantification of various organs at 24 h after intravenous injection of IR-780 micelles. Each column represents the mean ± SD. The abbreviations indicate: H, heart; Li, liver; Sp, spleen; Lu, lung; K, kidney; and In, intestine.

The spatial distribution of temperatures in the tumors of mice treated with PTT mediated by IR-780 micelles was observed with a thermal imaging camera (Thermo Shot F30, NEC Avio Infrared Technologies Co., Ltd.) (Figure 6C). Excluding the region exposed to NIR irradiation, the maximum body temperature was about 36 °C, corresponding to the normal body temperature of mice. For tumor regions treated with IR-780 micelles and exposed to NIR irradiation, the temperature along the scan line was quantitated, and the maximum tumor temperature increased to 56.6 °C (Figure 6D), which was similar to the temperature measured by the thermocouple needle.

We investigated how effectively PTT using IR-780 micelles on HCT-116 tumors in nude mice reduced tumor growth *in vivo* (Figure 7). Control tumors treated with PBS, only the NIR irradiation, or only IR-780 micelles grew rapidly and uniformly, with no statistically significant differences in final tumor sizes (P = 0.24). This indicated that tumor growth was not affected by either IR-780 micelles or NIR irradiation alone. In contrast, when the tumor volume was measured 27 days after PTT mediated by IR-780 micelles, it was reduced (mean tumor volume 271 ± 168 mm^3) compared with control tumors (1556 ± 216 mm^3) and TGI was 82.6% ($P < 0.01$).

Body weight loss was used as a measure of treatments-induced toxicity (Figure 7B). The body weights of both control and treatment groups were monitored throughout the experimental period, and mice that lost over 20% of their original body weight were sacrificed. By day 27, the control groups treated with

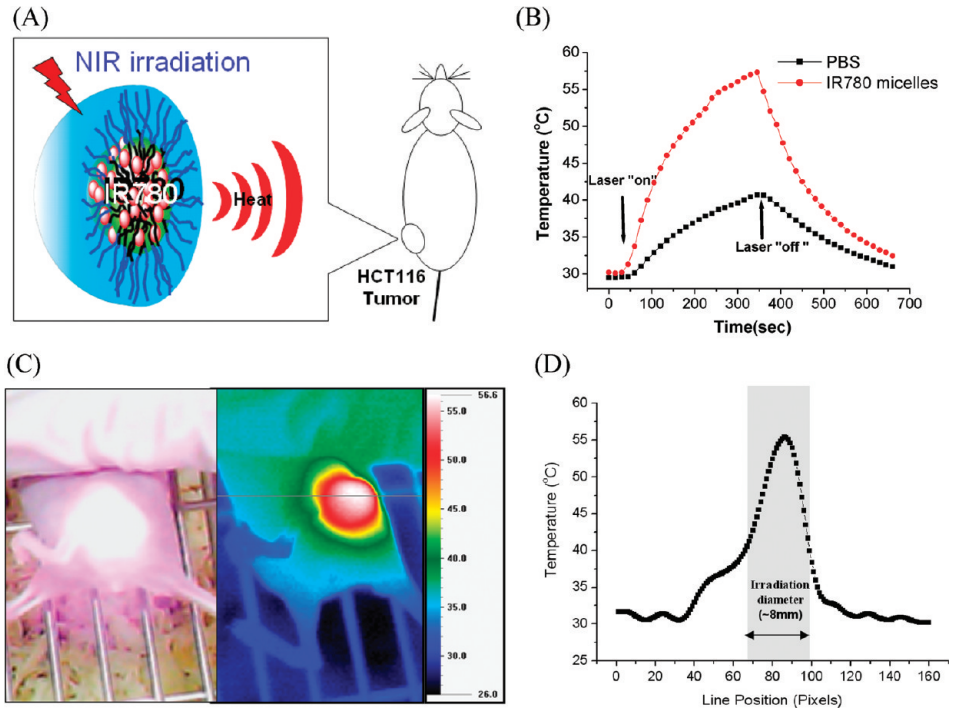

Figure 6. (A) Schematic diagram illustrating the photothermal therapy of IR-780 micelles following NIR light irradiation. (B) Intratumoral temperature profile during IR-780 micelle-mediated photothermal therapy was measured as a function of time with thermocouple needles inserted in the center of tumor while the tumor region was irradiated by the 1.8W/cm^2 NIR laser for 5 min. (C) Infrared thermographic map of the HCT-116 tumor treated with IR-780 micelles was measured with a thermal camera after NIR irradiation. (D) Temperature along the scan line in the corresponding thermal images in panel C was quantified, with the shaded region corresponding to the tumor region exposed to NIR light.

PBS or only the NIR irradiation gradually had increased their body weights by 6−11%, and those treated with the IR-780 micelles increased by 7%. These values were not significantly different between the control groups, which suggested that the dye dose was reasonably well-tolerated. It has been reported that heptamethine indocyanine dyes, such as IR-780 iodide and IR-783, had no systemic toxicity in normal C-57BL/6 mice and did not affect body weights of the mice as described previously.[21,46] No abnormal histopathology was seen in vital organs harvested from mice at the time of sacrifice. Intravenous injection with 100 nmol of IR-780 iodide, which was ~2.7 times higher than the dose we used in our *in vivo* studies, did not cause systemic toxicity.[46] Mice treated with IR-780 micelles plus NIR irradiation lost 4% of their weight at day 27. This weight loss was not significantly different from the control groups, indicating that photothermal therapy mediated by IR-780 micelles did not result in unacceptable toxicity.

To further determine the effect of IR-780 micelle-mediated photothermal therapy *in vivo*, subcutaneously, tumors underwent immunohistochemical analysis (Figure 8). Tumor tissues stained with hematoxylin and eosin had different tissue morphologies between treatment groups. As shown in Figure 8A, common markers of thermal damage in tumors treated with PTT mediated by IR-780 micelles plus NIR irradiation, such as coagulation, vacuolation, and loss of nuclear staining as described previously, were identified.[1] The sections were stained with nicotinamide adenine dinucleotide phosphate (NADPH)-diaphorase staining for the assessment of tissue viability. Necrotic tissue shows loss of NADPH-diaphorase activity.[47] The immunohistochemical analysis revealed that tumors treated with NIR irradiation alone had limited loss of NADPH-diaphorase activity at the surface of tumor, which was proximal to the incident laser (as shown in Figure 8A and Supporting Information Figure SI-6B). It is in good agreement with theoretical and experimental data published elsewhere.[1] Maximal temperature changes were found to occur ~1 mm beneath the apical surface. This behavior may be the product of higher photon densities in this region, which is a phenomenon often seen in highly scattering mediums like tissue. In contrast, tumors treated with IR-780 micelle-mediated PTT had prominent necrosis and vacuolation. Necrotic features caused by the loss of NADPH-diaphorase activity were observed at the interior of the tumors. The maximum treatable depths of IR-780 micelle-mediated PTT appeared to be ~5−6 mm in this study (as shown in Supporting Information Figure SI-6C), which was in agreement with experimental data published elsewhere.[1] These results indicate that NIR irradiation induced irreversible

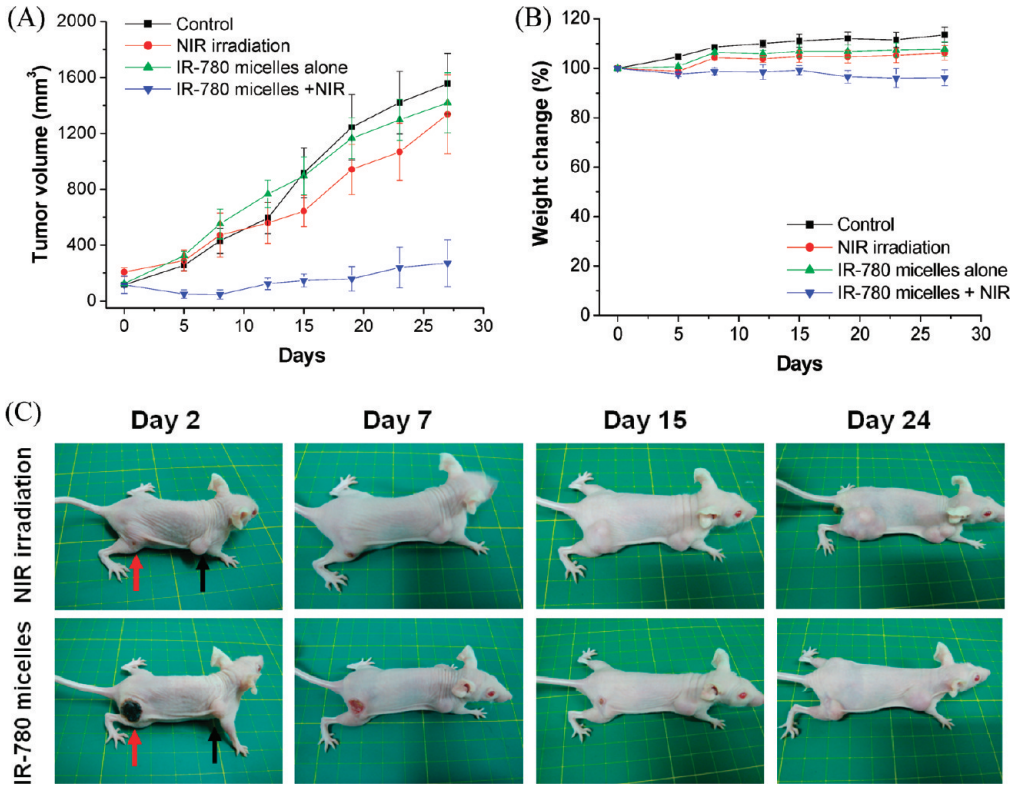

Figure 7. Effects of PTT mediated by IR-780 micelles in mice bearing HCT-116 tumor were measured. (A) Tumor volumes and (B) body weights were measured during the 27 day evaluation period in mice treated with PBS (control), NIR irradiation alone, IR-780 micelles alone, or IR-780 micelles plus NIR irradiation. Data indicate means and standard errors. (C) Representative mice treated with NIR irradiation alone or with IR-780 micelles equivalent to 1.25 mg/kg and 1.8 w/cm^2 NIR irradiation for 5 min were photographed over days 2−24. The red and black arrows indicate the NIR irradiation site and no NIR irradiation, respectively.

tissue damage mainly in the IR-780 micelle-treated tumor tissue.

Proliferating cell nuclear antigen (PCNA) immunolocalization can be used as an index of cell proliferation and may define the extent of departure from normal growth control.[48] The PBS control tumors had a mean of 151.5 ± 11.3 PCNA positive cells, and the tumors treated only with the NIR irradiation had a mean of 135.7 ± 5.8 (Figure 8B), which were not significantly between these two groups. The tumors treated with PTT mediated by IR-780 micelles plus NIR irradiation had decreased cell proliferation as detected by PCNA expression (mean ± SD = 48.4 ± 4.5) in the viable, non-necrotic regions (Figure 8B). Their cell proliferation was significantly lower than those treated with only NIR irradiation or with PBS (both $P < 0.01$), so combining NIR irradiation with IR-780 micelles reduced the number of proliferating cells within the subcutaneous tumors (Figure 8A,B).

Apoptotic cells in each treatment were identified by the terminal deoxynucleotidyl transferase dUTP nick end labeling (TUNEL) method. TUNEL is a method for detecting DNA fragmentation, which results from apoptotic signaling cascades, by labeling the terminal end of nucleic acids.[49] The PBS control group tumors had a mean of 9.3 ± 2.6 apoptotic cells, and those tumors treated only with NIR irradiation had a mean of 14.6 ± 3.2. The viable, non-necrotic regions in tumors treated with PTT mediated by IR-780 micelles plus NIR irradiation had more apoptotic tumor cells (mean ± SD = 98.2 ± 10.8) than either control group (for both, $P < 0.01$).

Since HSPs are induced by temperatures above 43 °C, they serve as endogenous markers of thermal stress.[50] Tumors treated only with PBS had minimal expression of HSPs, while those treated with only NIR irradiation had more HSP90 expression induced in the viable, non-necrotic regions of tumors, which were close to the incident laser (Figure 8). Tumors treated with PTT mediated by IR-780 micelles plus NIR irradiation had enough temperature elevation to induce necrosis at the inner of tumor, which prevented the induction of HSPs, though the viable tumor surrounding the necrotic region did have induced HSPs. These results suggest that PTT mediated by IR-780 micelles plus NIR irradiation can extend the depth of thermal therapy of tumors, resulting in inner necrosis and peripheral expression of HSPs. Measuring HSPs can also demarcate thermally treated regions[50] since HSPs allow cells to adapt to gradual changes in their environment and to survive conditions that would otherwise be lethal through

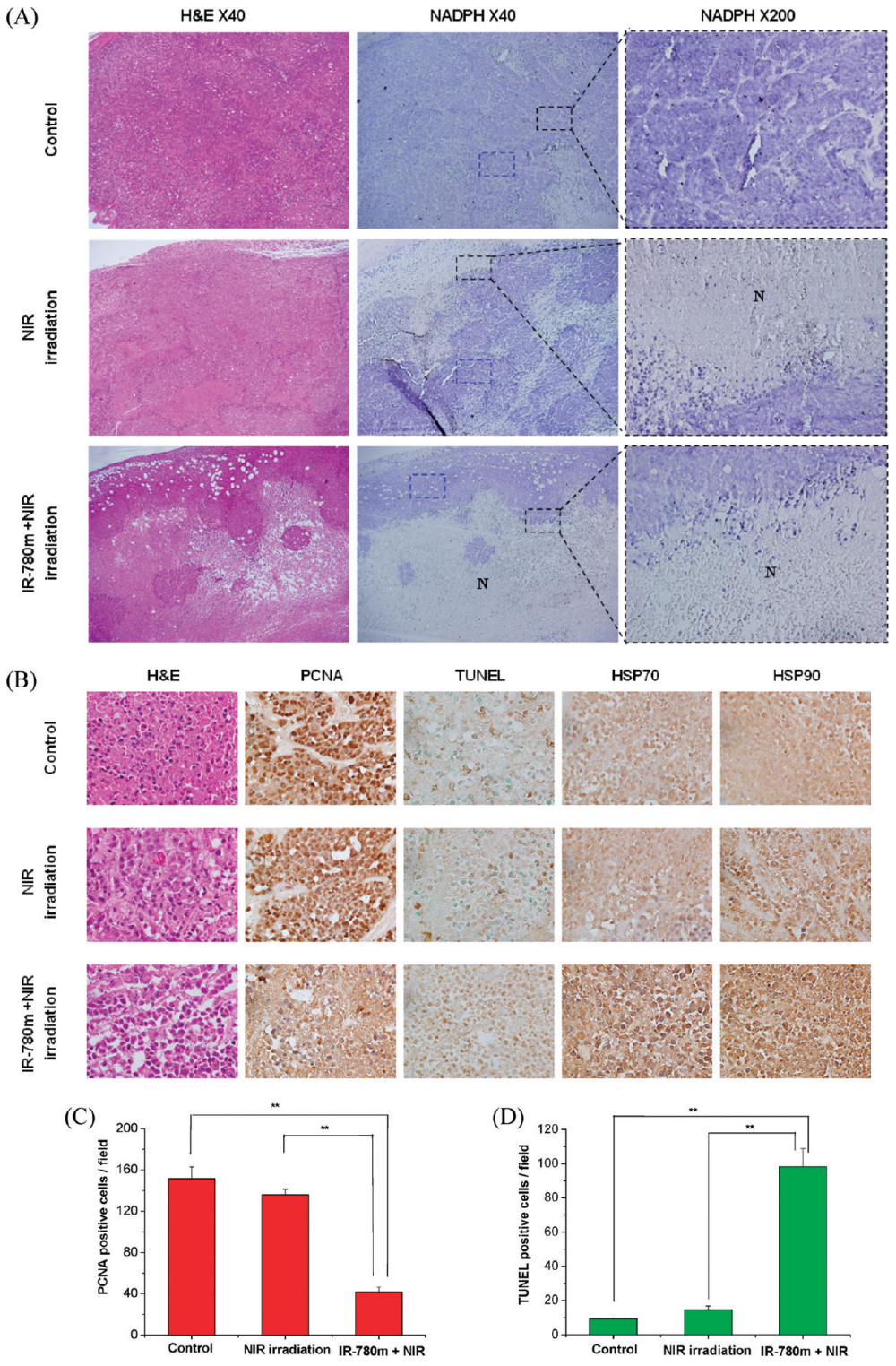

Figure 8. Histological and immunohistochemical analysis in HCT-116 xenograft tumors treated with IR-780 micelle-mediated photothermal therapy. (A) Tumor sections were analyzed by hematoxylin and eosin (H&E) staining, NADPH-diaphorase staining (NADPH). More necrotic (N) tissue on the interior of the tumors was present when the tumors were treated with the combination of IR-780 micelles and NIR irradiation, which indicates the loss of NADPH-diaphorase activity. (B) Immunohistochemical staining of PCNA, TUNEL, HSP70, and HSP90 from the blue dotted squares in panel A. (C) Cellular proliferation was quantified by assessing the number of PCNA-positive cells per field at 200× magnification, and (D) apoptotic cells were quantified by the TUNEL method at 200× magnification. The results represent the mean ± SD in 10 distinct regions from examining three tumors per group. The double star (**) indicates $P < 0.01$.

suppressing apoptosis and enhancing resistance to therapies.[51] Thus, measuring HSPs may aid in future searches for optimal conditions for PTT mediated by IR-780 micelles.

CONCLUSIONS

We have prepared and characterized IR-780 iodide-loaded micelles, which both acted as NIR contrast agents for optical imaging and were labeled with the radionuclide rhenium-188 (^{188}Re) for nuclear imaging. We demonstrated that the NIR dye, IR-780 iodide, could serve as a photosensitizing agent for photothermal therapy of cancer since using IR-780 micelles to generate heat upon NIR irradiation resulted in thermal destruction of colon cancer both *in vitro* and *in vivo*. Measurements of the viable regions around necrotic regions of tumors found that these treatments decreased the cell proliferation as measured by PCNA expression, increased apoptotic cells as measured by TUNEL, and increased the expression of HSPs. These results indicate that irreversible tissue damage was induced by PTT mediated by the IR-780 micelles plus NIR irradiation in treated tumors. This platform permits image-guided drug delivery. The tumor accumulation, intratumoral distribution, and kinetics of the drug can be monitored in real-time. This platform allows diagnosis and therapeutics to be combined in optical/nuclear imaging and PTT. The ^{188}Re-labeled IR-780 micelles potentially offer multifunctional modalities for the near-infrared (NIR) fluorescence and nuclear imaging and for photothermal therapy of cancer.

MATERIALS AND METHODS

Synthesis of mPEG-*b*-PCL and DTPA-PEG-b-PCL. Methoxy poly(ethylene glycol)-*block*-poly(ε-caprolactone) (mPEG-*b*-PCL) and fluorenylmethyloxycarbonyl-amino-poly(ethylene glycol)-*block*-poly(ε-caprolactone) (Fmoc-NH-PEG-*b*-PCL) amphiphilic block copolymers were synthesized by ring-opening polymerization of ε-caprolactone at 140 °C overnight in the presence of mPEG-OH (MW = 5000) and Fmoc-NH-PEG-OH (MW = 5000) as a macroinitiator under stannous octoate (SnOct) catalysis[27,28] (Figure 1). The Fmoc-NH-PEG-*b*-PCL was deprotected by stirring Fmoc-NH-PEG-*b*-PCL in 2 mL of 20% piperidine in DMF for 2 h at room temperature.[36] Then, the NH_2-PEG-*b*-PCL was purified by dialysis against water for 7 days, with the deionized water being changed twice per day. The DTPA-PEG-*b*-PCL was prepared by conjugating DTPA dianhydride with the amino group of N_2H-PEG-*b*-PCL as described previously.[37] The details of experimental section are presented in the Supporting Information. The molecular weights of the synthesized polymers were characterized by ^{1}H NMR (Bruker Avance 500 MHz FT-NMR) using deuterated chloroform ($CDCl_3$) as the solvent and gel permeation chromatography (GPC) using Waters 510 pump equipped with a Waters 410 differential refractometer. Tetrahydrofuran (THF) was used as the eluent at a flow rate of 1.0 mL/min. Calibration used monodispersed polystyrene standards. The DTPA conjugation efficiency was evaluated by the radiolabeling yields of ^{188}Re-DTPA-PEG-*b*-PCL, as analyzed by instant thin layer chromatography (ITLC), and by calculating the relative amounts of ^{188}Re-DTPA-PEG-*b*-PCL and free ^{188}Re-DTPA (R_f ^{188}Re-DTPA-PEG-*b*-PCL= 0; R_f ^{188}Re-DTPA= 1).

Preparing IR-780 Micelles and IR-780/DTPA Micelles. We prepared IR-780 micelles and IR-780-loaded/DTPA micelles (IR-780/DTPA micelles) by the cosolvent evaporation method.[27] Briefly, a mixture of 10−40 mg of mPEG-*b*-PCL was dissolved in acetone with 2 mg of IR-780 iodide dye (*D*/*P* = 1/5−1/20), or 36 mg of mPEG-*b*-PCL and 4 mg of DTPA-PEG-*b*-PCL in a ratio of 9:1 were dissolved in acetone with 2 mg of IR-780 dye (D/P was 1:20). These mixtures were added to saline while stirring at a speed of 550 rpm. The organic solvent was evaporated, while the solution was stirred overnight. Then, the solution was filtered through a 0.45 μm sterile filter (Millex GS, Millipore, Bedford, MA, USA) to remove non-incorporated drug crystals and copolymer aggregates. The concentration of IR-780 iodide was determined with a spectrophotometer using a quartz cell with a 1 cm path length at 786 nm. The drug encapsulation efficiency is the amount of drug encapsulated divided by the amount of drug added multiplied by 100%.

Preparing ^{188}Re-Labeled IR-780 Micelles. The ^{188}Re with DTPA micelles were labeled by reacting a mixture of 1 mL of DTPA micelles, 100 μL of ^{188}Re-perrhenate ($^{188}ReO_4$, ~37 MBq), and 5 mg of stannous chloride for 2 h at 37 °C.[52,53] The radiolabeling yields of ^{188}Re-DTPA micelles were determined by ITLC using silica gel as the stationary phase and normal saline as the mobile phase. The chromatograms were analyzed by a radio thin layer chromatography imaging scanner (AR2000, Bioscan, Washington, DC, USA).

Characterizing IR-780 Micelles. The mean diameter and polydispersity index (PDI) of the micelles were characterized with a Delsa Nano Particle Analyzer (Beckman Coulter, Fullerton, CA). The morphology of the micelles was observed by H-7650 transmission electron microscopy (TEM, Hitachi Ltd., Tokyo, Japan). The absorptions of the IR-780 iodide dissolved in 0.15 M NaCl buffer and of IR-780 micelles dispersed in phosphate buffer saline (PBS) were measured on a UV−vis spectrophotometer (BioMate 3S, Thermo Electron Corporation, Hudson, NH, USA) with a quartz thermostatted cell with a 1 cm path length. The temperature profile of the IR-780 micelles during NIR irradiation was analyzed in a 24-well plate with a thermocouple needle. A total of 1 mL of ~100 μg/mL IR-780 micelles was added to one of the wells, the well was irradiated by the NIR laser at 1.8 W/cm^2, and the temperature of the well was measured continuously over 5 min.

***In Vitro* Cytotoxicity.** The HCT-116 cells were incubated in media containing different concentrations of IR-780 micelles for 3 h and washed with PBS. Next, the cells were treated for 10 min with a laser diode with a wavelength of 808 nm at a power density of 0.6 W/cm^2. After the irradiation, the cells were stained for 30 min with 2 μM calcein-AM and 2 μM propidium idodide (PI) prior to imaging. Cell viability was visually determined with an X51 Olympus fluorescence microscope (Olympus Optical Co., Tokyo, Japan).

The cytotoxicity of treating HCT-116 cells with IR-780 micelles and NIR irradiation was additionally determined. The HCT-116 cells were first seeded onto 96-well plates at a density of 10 000 cells per well and cultured. After 24 h, the cells were incubated in media with different concentrations of IR-780 micelles for 3 h and then washed with PBS. Next, the cells were treated with a laser diode with a wavelength of 808 nm at a power density of 0.6 W/cm^2 for 10 or 20 min. Cell viability was determined with the MTT assay and a scanning multiwell ELISA reader (Microplate Autoreader EL311, Bio-Tek Instruments Inc., Winooski, VT, USA). The fraction of live cells was calculated by dividing the mean optical density obtained from treated cells by the mean optical density from untreated control cells.

Biodistribution of ^{188}Re-Labeled IR-780 Micelles and IR-780 Iodide by Micelle Formulas. Female BALB/c athymic (nut/nut) mice that were 5−6 weeks old were purchased from the National Laboratory Animal Center (Taipei, Taiwan). Tumors were initially established by subcutaneously injecting a mixture of 1×10^6 HCT-116 cells, matrigel, and DMEM. Tumor sizes and body weights were measured every 3 days for the duration of the experiment. Tumor volume was calculated as $\pi/6ab^2$, where *a* is the length and *b* is the width of the tumor.

Mice received an intravenous injection of ^{188}Re-labeled IR-780 micelles, equivalent to 22 MBq of ^{188}Re, when the tumors reached a volume of 150 to 200 mm^3. The distribution of ^{188}Re-labeled IR-780 micelles in the mice bearing HCT-116 tumors was

evaluated by microSPECT/CT images at 1, 4, and 24 h after the micelles were intravenously injected.

The mice were sacrificed by cervical vertebra dislocation at 24 and 96 h after the intravenous administration of ^{188}Re-labeled IR-780 micelles. The plasma, tumor, and normal tissue were collected, and the uptake of radioactivity was measured by a γ counter. The distribution data were expressed as the percentage of injected dose (ID).

The biodistribution of IR-780 iodide was studied by injecting 1.25 mg/kg IR-780 micelles intravenously through a tail vein of mice bearing HCT-116 tumors and was imaged 1, 4, 24, 48, and 96 h after the injection with an IVIS imaging system (Xenogen, Alameda, CA, USA). The details of experiment are presented in the Supporting Information. Dye accumulation and retention in tumors was evaluated by calculating the contrast index (CI) values.[54] The tumor-bearing mice were sacrificed 48 h after the IR-780 micelles were injected, and then the tumor, heart, liver, spleen, lung, kidneys, and intestine were harvested for isolated organ imaging to estimate the tissue distribution of IR-780 micelles.

Temperature Measurements. The intratumoral temperature increases upon NIR irradiation were determined by injecting 1.25 mg/kg IR-780 micelles through a tail vein into mice bearing HCT-116 tumors. Control mice were injected with 100 μL of empty micelles (equivalent to 25 mg/kg). The temperatures of the tumor tissues during NIR irradiation were measured 96 h after the injections with thermocouple needles (127 μm diameter, T-type, copper−constantan thermocouple, Omega Engineering, Stamford, CT) connected to a data acquisition system (TC-2190, National Instruments, Austin, TX). First, the 23 gauge needles intratumorally injected into the center of tumor about 3−4 mm in depth. Next, the thermocouples were inserted into the tumor through the 23 gauge needles, while the tumor region was exposed to 1.8 W/cm^2 NIR light for 5 min with a laser diode (λ = 808 nm). All data were analyzed with Matlab (Mathworks, Natick, MA, USA). The distribution of tumoral temperature after NIR irradiation was examined with an IR thermographic camera (F30s, NEC Avio Infrared Technologies Co., Ltd., Tokyo, Japan) in the mice treated with the IR-780 micelles.

Antitumor Efficacy of the IR-780 Micelles upon NIR Irradiation. Treatments were started when the tumors reached a volume of 100 to 150 mm^3. The mice were divided into groups of five mice each that were treated with the PBS control, the NIR irradiation alone, the IR-780 micelles, or the combination of IR-780 micelles and NIR irradiation. The IR-780 micelles were administered *via* tail vein injections at doses equivalent to 1.25 mg/kg of IR-780 iodide, and 96 h after the micelles were administered was designated as day 0. On day 0, the tumors were exposed to the NIR laser with a spot size of 5 mm at 1.8 W/cm^2 for 5 min. The tumor size and change in body weight of each mouse were recorded. The percentage of tumor growth inhibition (TGI) was calculated from the relative tumor volume on day 27 and is presented as percent reduction in the mean tumor volume in experimental groups compared with saline-treated control groups.

Necropsy and Immunohistochemical Analysis. After the mice were sacrificed, the tumors were excised and fixed in formalin and embedded in paraffin for immunohistochemical staining and for hematoxylin and eosin staining. The tumor sections, which were paraffin-embedded and 5 mm thick, were analyzed by immunohistochemical staining for proliferating cell nuclear antigen (PCNA), heat shock protein 70 (HSP70), and heat shock protein 90 (HSP90). Consecutive sections were incubated overnight at 4 °C with antibodies specific for HSP70 (rabbit antihuman, diluted 1:50, Cell Signaling Technology Inc., Danvers, MA, USA), HSP90 (rabbit antihuman, diluted 1:50, Cell Signaling), and PCNA (mouse anti-PCNA, clone PC 10, Sigma). The immunostaining was applied and visualized by useing Histostain-Plus kits (Zymed Laboratories, Inc., San Francisco, CA, USA). The terminal deoxynucleotidyl transferase dUTP nick end labeling (TUNEL) assay was carried out with the DeadEnd Colorimetric TUNEL System (Promega, Fitchburg, WI, USA). The NADPH-diaphorase staining was carried out to demonstrate the necrosis as described previously with minor modifications.[47] Tissue viability was analyzed by reacting the samples for 20 min at room temperature with NADPH-diaphorase reaction solution. The details of the experiment are presented in the Supporting Information.

Statistical Analysis. All data are expressed as mean ± standard deviation. The significance of difference in this study between groups was analyzed by the *t*-test. A value of $P < 0.05$ was considered statistically significant.

Acknowledgment. We are grateful to the staff of TC5 Bio-Image Tools, Technology Commons, College of Life Science, NTU, for their help with transmission electron microscopy. This research was funded by the National Science Council of the Republic of China (NSC99-2218-E-002-011-) and the Department of Health, Executive Yuan, Taiwan, ROC (research project nos. DOH100-TD-N-111-005).

Supporting Information Available: (1) ^{1}H NMR spectra of mPEG$_{5k}$-PCL$_{10k}$ and Fmoc-PEG$_{5k}$-PCL$_{10k}$ copolymers; (2) GPC chromatograms for Fmoc-NH-PEG-OH and Fmoc-NH-PEG-*b*-PCL copolymers; (3) radiochemical purity analysis of the crude labeled mixture of ^{188}Re-DTPA-PEG-*b*-PCL; (4) static light scattering (SLS) of IR-780 micelles; (5) radiochemical purity analysis of the ^{188}Re-DTPA-micelles; (6) histopathological analysis of HCT-116 xenograft tumors treated with NIR irradiation alone, or IR-780 micelles + NIR irradiation. This material is available free of charge *via* the Internet at http://pubs.acs.org.

REFERENCES AND NOTES

1. Hirsch, L. R.; Stafford, R. J.; Bankson, J. A.; Sershen, S. R.; Rivera, B.; Price, R. E.; Hazle, J. D.; Halas, N. J.; West, J. L. Nanoshell-Mediated Near-Infrared Thermal Therapy of Tumors under Magnetic Resonance Guidance. *Proc. Natl. Acad. Sci. U.S.A.* **2003**, *100*, 13549–13554.
2. Gobin, A. M.; Lee, M. H.; Halas, N. J.; James, W. D.; Drezek, R. A.; West, J. L. Near-Infrared Resonant Nanoshells for Combined Optical Imaging and Photothermal Cancer Therapy. *Nano Lett.* **2007**, *7*, 1929–1934.
3. Gazelle, G. S.; Goldberg, S. N.; Solbiati, L.; Livraghi, T. Tumor Ablation with Radio-Frequency Energy1. *Radiology* **2000**, *217*, 633–646.
4. Hilger, I.; Hiergeist, R.; Hergt, R.; Winnefeld, K.; Schubert, H.; Kaiser, W. A. Thermal Ablation of Tumors Using Magnetic Nanoparticles: An *In Vivo* Feasibility Study. *Invest. Radiol.* **2002**, *37*, 580–586.
5. Schmitz, A. C.; Gianfelice, D.; Daniel, B. L.; Mali, W.; van den Bosch, M. Image-Guided Focused Ultrasound Ablation of Breast Cancer: Current Status, Challenges, and Future Directions. *Eur. Radiol.* **2008**, *18*, 1431–1441.
6. Streitparth, F.; Knobloch, G.; Balmert, D.; Chopra, S.; Rump, J.; Wonneberger, U.; Philipp, C.; Hamm, B.; Teichgraber, U. Laser-Induced Thermotherapy (LITT)-Evaluation of a Miniaturised Applicator and Implementation in a 1.0-T High-Field Open MRI Applying a Porcine Liver Model. *Eur. Radiol.* **2010**, *20*, 2671–2678.
7. Vogl, T. J.; Naguib, N. N. N.; Eichler, K.; Lehnert, T. Ackermann, H.; Mack, M. G. Volumetric Evaluation of Liver Metastases after Thermal Ablation: Long-Term Results Following MR-Guided Laser-Induced Thermotherapy. *Radiology* **2008**, *249*, 865–871.
8. Fisher, J. W.; Sarkar, S.; Buchanan, C. F.; Szot, C. S.; Whitney, J.; Hatcher, H. C.; Torti, S. V.; Rylander, C. G.; Rylander, M. N. Photothermal Response of Human and Murine Cancer Cells to Multiwalled Carbon Nanotubes after Laser Irradiation. *Cancer Res.* **2010**, *70*, 9855–9864.
9. Wu, W. T.; Shen, J.; Banerjee, P.; Zhou, S. Q. Core−Shell Hybrid Nanogels for Integration of Optical Temperature-Sensing, Targeted Tumor Cell Imaging, and Combined Chemo-Photothermal Treatment. *Biomaterials* **2010**, *31*, 7555–7566.
10. Skirtach, A. G.; Dejugnat, C.; Braun, D.; Susha, A. S.; Rogach, A. L.; Parak, W. J.; Mohwald, H.; Sukhorukov, G. B. The Role of Metal Nanoparticles in Remote Release of Encapsulated Materials. *Nano Lett.* **2005**, *5*, 1371–1377.

11. Chen, C. L.; Kuo, L. R.; Chang, C. L.; Hwu, Y. K.; Huang, C. K.; Lee, S. Y.; Chen, K.; Lin, S. J.; Huang, J. D.; Chen, Y. Y. *In Situ* Real-Time Investigation of Cancer Cell Photothermolysis Mediated by Excited Gold Nanorod Surface Plasmons. *Biomaterials* **2010**, *31*, 4104–4112.
12. Huang, X.; El-Sayed, I. H.; Qian, W.; El-Sayed, M. A. Cancer Cell Imaging and Photothermal Therapy in the Near-Infrared Region by Using Gold Nanorods. *J. Am. Chem. Soc.* **2006**, *128*, 2115–2120.
13. Choi, W. I.; Kim, J. Y.; Kang, C.; Byeon, C. C.; Kim, Y. H.; Tee, G. Tumor Regression *In Vivo* by Photothermal Therapy Based on Gold-Nanorod-Loaded, Functional Nanocarriers. *ACS Nano* **2011**, *5*, 1995–2003.
14. Skirtach, A. G.; Antipov, A. A.; Shchukin, D. G.; Sukhorukov, G. B. Remote Activation of Capsules Containing Ag Nanoparticles and Ir Dye by Laser Light. *Langmuir* **2004**, *20*, 6988–6992.
15. Bardhan, R.; Chen, W. X.; Perez-Torres, C.; Bartels, M.; Huschka, R. M.; Zhao, L. L.; Morosan, E.; Pautler, R. G.; Joshi, A.; Halas, N. J. Nanoshells with Targeted Simultaneous Enhancement of Magnetic and Optical Imaging and Photothermal Therapeutic Response. *Adv. Funct. Mater.* **2009**, *19*, 3901–3909.
16. Chen, W. R.; Adams, R. L.; Higgins, A. K.; Bartels, K. E.; Nordquist, R. E. Photothermal Effects on Murine Mammary Tumors Using Indocyanine Green and an 808-nm Diode Laser: An *In Vivo* Efficacy Study. *Cancer Lett.* **1996**, *98*, 169–173.
17. Yu, J.; Javier, D.; Yaseen, M. A.; Nitin, N.; Richards-Kortum, R.; Anvari, B.; Wong, M. S. Self-Assembly Synthesis, Tumor Cell Targeting, and Photothermal Capabilities of Antibody-Coated Indocyanine Green Nanocapsules. *J. Am. Chem. Soc.* **2010**, *132*, 1929–1938.
18. Weissleder, R. A Clearer Vision for *In Vivo* Imaging. *Nat. Biotechnol.* **2001**, *19*, 316–317.
19. Roggan, A.; Friebel, M.; Dorschel, K.; Hahn, A.; Muller, G. Optical Properties of Circulating Human Blood in the Wavelength Range 400−2500 nm. *J. Biomed. Opt.* **1999**, *4*, 36–46.
20. Rao, J. H.; Dragulescu-Andrasi, A.; Yao, H. Q. Fluorescence Imaging *In Vivo*: Recent Advances. *Curr. Opin. Biotechnol.* **2007**, *18*, 17–25.
21. Yang, X. J.; Shi, C. M.; Tong, R.; Qian, W. P.; Zhau, H. E.; Wang, R. X.; Zhu, G. D.; Cheng, J. J.; Yang, V. W.; Cheng, T. M.; *et al.* Near IR Heptamethine Cyanine Dye-Mediated Cancer Imaging. *Clin. Cancer Res.* **2010**, *16*, 2833–2844.
22. Zhang, C.; Liu, T.; Su, Y.; Luo, S.; Zhu, Y.; Tan, X.; Fan, S.; Zhang, L.; Zhou, Y.; Cheng, T.; *et al.* A Near-Infrared Fluorescent Heptamethine Indocyanine Dye with Preferential Tumor Accumulation for *In Vivo* Imaging. *Biomaterials* **2010**, *31*, 6612–6617.
23. Gref, R.; Minamitake, Y.; Peracchia, M. T.; Trubetskoy, V.; Torchilin, V.; Langer, R. Biodegradable Long-Circulating Polymeric Nanospheres. *Science* **1994**, *263*, 1600–1603.
24. Kwon, G. S.; Okano, T. Polymeric Micelles as New Drug Carriers. *Adv. Drug Delivery Rev.* **1996**, *21*, 107–116.
25. Savic, R.; Luo, L. B.; Eisenberg, A.; Maysinger, D. Micellar Nanocontainers Distribute to Defined Cytoplasmic Organelles. *Science* **2003**, *300*, 615–618.
26. Yasugi, K.; Nagasaki, Y.; Kato, M.; Kataoka, K. Preparation and Characterization of Polymer Micelles from Poly(ethylene glycol)-Poly(D,L-lactide) Block Copolymers as Potential Drug Carrier. *J. Controlled Release* **1999**, *62*, 89–100.
27. Peng, C. L.; Shieh, M. J.; Tsai, M. H.; Chang, C. C.; Lai, P. S. Self-Assembled Star-Shaped Chlorin-Core Poly(ε-caprolactone)-Poly(ethylene glycol) Diblock Copolymer Micelles for Dual Chemo-Photodynamic Therapies. *Biomaterials* **2008**, *29*, 3599–3608.
28. Peng, C. L.; Lai, P. S.; Lin, F. H.; Wu, S. Y. H.; Shieh, M. J. Dual Chemotherapy and Photodynamic Therapy in an HT-29 Human Colon Cancer Xenograft Model Using SN-38-Loaded Chlorin-Core Star Block Copolymer Micelles. *Biomaterials* **2009**, *30*, 3614–3625.
29. Shieh, M. J.; Peng, C. L.; Chiang, W. L.; Wang, C. H.; Hsu, C. Y.; Wang, S. J. J.; Lai, P. S. Reduced Skin Photosensitivity with *meta*-Tetra(hydroxyphenyl)chlorin-Loaded Micelles Based on a Poly(2-ethyl-2-oxazoline)-*B*-Poly(D,L-lactide) Diblock Copolymer *In Vivo*. *Mol. Pharmaceutics* **2010**, *7*, 1244–1253.
30. Maruyama, K.; Ishida, O.; Takizawa, T.; Moribe, K. Possibility of Active Targeting to Tumor Tissues with Liposomes. *Adv. Drug Delivery Rev.* **1999**, *40*, 89–102.
31. Lee, H.; Hoang, B.; Fonge, H.; Reilly, R.; Allen, C. *In Vivo* Distribution of Polymeric Nanoparticles at the Whole-Body, Tumor, and Cellular Levels. *Pharm. Res.* **2010**, *27*, 2343–2355.
32. Hoang, B.; Lee, H.; Reilly, R. M.; Allen, C. Noninvasive Monitoring of the Fate of 111in-Labeled Block Copolymer Micelles by High Resolution and High Sensitivity Micro-SPECT/CT Imaging. *Mol. Pharmaceutics* **2009**, *6*, 581–592.
33. Pressly, E. D.; Rossin, R.; Hagooly, A.; Fukukawa, K.-i.; Messmore, B. W.; Welch, M. J.; Wooley, K. L.; Lamm, M. S.; Hule, R. A.; Pochan, D. J.; *et al.* Structural Effects on the Biodistribution and Positron Emission Tomography (PET) Imaging of Well-Defined ^{64}Cu-Labeled Nanoparticles Comprised of Amphiphilic Block Graft Copolymers. *Biomacromolecules* **2007**, *8*, 3126–3134.
34. Shokeen, M.; Fettig, N. M.; Rossin, R. Synthesis, *In Vitro* and *In Vivo* Evaluation of Radiolabeled Nanoparticles. *Q. J. Nucl. Med. Mol. Imaging* **2008**, *52*, 267–277.
35. Hamoudeh, M.; Kamleh, M. A.; Diab, R.; Fessi, H. Radionuclides Delivery Systems for Nuclear Imaging and Radiotherapy of Cancer. *Adv. Drug Delivery Rev.* **2008**, *60*, 1329–1346.
36. Zhang, N.; Chittasupho, C.; Duangrat, C.; Siahaan, T. J.; Berkland, C. PLGA Nanoparticle−Peptide Conjugate Effectively Targets Intercellular Cell-Adhesion Molecule-1. *Bioconjugate Chem.* **2007**, *19*, 145–152.
37. Fonge, H.; Lee, H.; Reilly, R. M.; Allen, C. Multifunctional Block Copolymer Micelles for the Delivery of ^{111}In to EGFR-Positive Breast Cancer Cells for Targeted Auger Electron Radiotherapy. *Mol. Pharmaceutics* **2009**, *7*, 177–186.
38. Maeda, H.; Wu, J.; Sawa, T.; Matsumura, Y.; Hori, K. Tumor Vascular Permeability and the EPR Effect in Macromolecular Therapeutics: A Review. *J. Controlled Release* **2000**, *65*, 271–284.
39. Monsky, W. L.; Fukumura, D.; Gohongi, T.; Ancukiewcz, M.; Weich, H. A.; Torchilin, V. P.; Yuan, F.; Jain, R. K. Augmentation of Transvascular Transport of Macromolecules and Nanoparticles in Tumors Using Vascular Endothelial Growth Factor. *Cancer Res.* **1999**, *59*, 4129–4135.
40. Litzinger, D. C.; Buiting, A. M. J.; Vanrooijen, N.; Huang, L. Effect of Liposome Size on the Circulation Time and Intraorgan Distribution of Amphipathic Poly(ethylene glycol)-Containing Liposomes. *Biochim. Biophys. Acta* **1994**, *1190*, 99–107.
41. Moghimi, S. M.; Hunter, A. C.; Murray, J. C. Long-Circulating and Target-Specific Nanoparticles: Theory to Practice. *Pharmacol. Rev.* **2001**, *53*, 283–318.
42. Kassab, K. Photophysical and Photosensitizing Properties of Selected Cyanines. *J. Photochem. Photobiol. B* **2002**, *68*, 15–22.
43. Cauchon, N.; Tian, H.; Langlois, R.; La Madeleine, C.; Martin, S.; Ali, H.; Hunting, D.; van Lier, J. E. Structure−Photodynamic Activity Relationships of Substituted Zinc Trisulfophthalocyanines. *Bioconjugate Chem.* **2004**, *16*, 80–89.
44. Poste, G.; Kirsh, R. Site-Specific (Targeted) Drug Delivery in Cancer-Therapy. *Bio-Technology* **1983**, *1*, 869–878.
45. Jang, B.; Park, J.-Y.; Tung, C.-H.; Kim, I.-H.; Choi, Y. Gold Nanorod−Photosensitizer Complex for Near-Infrared Fluorescence Imaging and Photodynamic/Photothermal Therapy *In Vivo*. *ACS Nano* **2011**, *5*, 1086–1094.
46. Zhang, C.; Wang, S.; Xiao, J.; Tan, X.; Zhu, Y.; Su, Y.; Cheng, T.; Shi, C. Sentinel Lymph Node Mapping by a Near-Infrared Fluorescent Heptamethine Dye. *Biomaterials* **2010**, *31*, 1911–1917.
47. Zuchini, R.; Huang, C. H.; Tsai, H. W.; Huang, S. C.; Lin, C. P.; Chen, C. Y.; Lee, G. B.; Lin, X. Z. Electromagnetic Thermoablation To Treat Thrombocytopenia in Cirrhotic and

Hypersplenic Rats. *J. Gastroenterol. Hepatol.* **2010**, *25*, 1578–1586.
48. Hall, P. A.; Levison, D. A.; Woods, A. L.; Yu, C. C. W.; Kellock, D. B.; Watkins, J. A.; Barnes, D. M.; Gillett, C. E.; Camplejohn, R.; Dover, R.; *et al.* Proliferating Cell Nuclear Antigen (PCNA) Immunolocalization in Paraffin Sections: An Index of Cell Proliferation with Evidence of Deregulated Expression in Some, Neoplasms. *J. Pathol.* **1990**, *162*, 285–294.
49. Gavrieli, Y.; Sherman, Y.; Ben-Sasson, S. A. Identification of Programmed Cell Death *In Situ via* Specific Labeling of Nuclear DNA Fragmentation. *J. Cell Biol.* **1992**, *119*, 493–501.
50. Burke, A.; Ding, X. F.; Singh, R.; Kraft, R. A.; Levi-Polyachenko, N.; Rylander, M. N.; Szot, C.; Buchanan, C.; Whitney, J.; Fisher, J.; *et al.* Long-Term Survival Following a Single Treatment of Kidney Tumors with Multiwalled Carbon Nanotubes and Near-Infrared Radiation. *Proc. Natl. Acad. Sci. U.S.A.* **2009**, *106*, 12897–12902.
51. Garrido, C.; Gurbuxani, S.; Ravagnan, L.; Kroemer, G. Heat Shock Proteins: Endogenous Modulators of Apoptotic Cell Death. *Biochem. Biophys. Res. Commun.* **2001**, *286*, 433–442.
52. Chen, Y.; Xiong, Q. F.; Yang, X. Q.; He, L.; Huang, Z. W. Evaluation of ^{188}Re-DTPA-Deoxyglucose as a Potential Cancer Radiopharmaceutical. *Am. J. Roentgenol.* **2010**, *194*, 761–765.
53. Hsieh, B. T.; Hsieh, J. F.; Tsai, S. C.; Lin, W. Y.; Huang, H. T.; Ting, G.; Wang, S. J. Rhenium-188-Labeled DTPA: A New Radiopharmaceutical for Intravascular Radiation Therapy. *Nucl. Med. Biol.* **1999**, *26*, 967–972.
54. Andreev, O. A.; Dupuy, A. D.; Segala, M.; Sandugu, S.; Serra, D. A.; Chichester, C. O.; Engelman, D. M.; Reshetnyak, Y. K. Mechanism and Uses of a Membrane Peptide That Targets Tumors and Other Acidic Tissues *In Vivo*. *Proc. Natl. Acad. Sci. U.S.A.* **2007**, *104*, 7893–7898.